Temporal and spatial changes in grassland transpiration detected using Landsat TM and ETM+ imagery

C.D. Holifield, S. McElroy, M.S. Moran, R. Bryant, T. Miura, and W.E. Emmerich

Abstract. The water deficit index (WDI) derived from Landsat imagery was used to detect temporal and spatial changes in grassland transpiration. The WDI, which estimates relative evapotranspiration rates based on meteorological data and the relation between surface reflectance and temperature, has been successfully applied over heterogeneous terrain with little a priori information. In this study, WDI was derived from a 10-year, Landsat-4 thematic mapper (TM), Landsat-5 TM, and Landsat-7 enhanced thematic mapper plus (ETM+) data series of the Walnut Gulch Experimental Watershed in Arizona during the summer monsoon period. Our study showed that measurements of surface reflectance and temperature from the three sensors could be combined without sacrificing product accuracy. WDI was correlated ($R^2 = 0.73$) with grassland transpiration measured by in situ instruments. Further, WDI varied temporally and spatially with variations in plant transpiration related to antecedent rainfall and slope aspect. WDI was compared with a measure of plant-available soil moisture (the antecedent retention index, ARI), which was derived from an hourly record of precipitation and runoff, obtained from rain gauges and flumes located in the watershed. Results showed that a nonlinear relation between WDI and ARI was significant but weak ($R^2 = 0.45$) and implied that WDI was the more sensitive indicator of vegetation condition. Ultimately, the WDI approach may be used as a viable tool to monitor grassland condition over heterogeneous regions.

Résumé. L'indice WDI (water deficit index) dérivé des images Landsat a été utilisé pour détecter les changements temporels et spatiaux de la transpiration dans les prairies. Le WDI, qui estime le taux d'évapotranspiration relative à partir des données météorologiques et de la relation entre la réflectance de surface et la température, a été appliqué avec succès au-dessus de reliefs hétérogènes avec peu d'informations a priori. Dans cette étude, le WDI a été dérivé d'une série de données TM (thematic mapper) de Landsat-4 et Landsat-5 et ETM+ de Landsat-7 acquises sur une période de dix ans au-dessus du bassin versant expérimental de Walnut Gulch (Walnut Gulch Experimental Watershed), en Arizona, durant la période de mousson d'été. Notre étude a démontré que les mesures de réflectance de surface et de température dérivées des trois capteurs pouvaient être combinées sans sacrifier la précision du produit. Le WDI était corrélé ($R^2 = 0,73$) avec la transpiration dans les prairies mesurée au moyen d'instruments in situ. De plus, le WDI variait temporellement et spatialement suivant les variations de la transpiration des plantes reliées à des précipitations antérieures ou au degré de pente. Le WDI a été comparé à une mesure de l'humidité du sol disponible à la plante (l'index ARI, antecedent retention index) dérivée d'enregistrements horaires de précipitation et de ruissellement acquis au moyen de pluviomètres et de canaux jaugeurs situés dans le bassin versant. Les résultats ont démontré qu'il existait une relation non-linéaire significative mais faible ($R^2 = 0,45$) entre le WDI et le ARI laissant supposer que le WDI constitue un indicateur plus sensible de la condition de la végétation. Éventuellement, l'approche WDI pourrait être utilisée comme outil viable pour le suivi des conditions des prairies dans des régions hétérogènes.
[Traduit par la Rédaction]

Introduction

Grasslands compose a substantial portion of the world's rangeland ecosystem. They are a significant food source for wild and domestic animals and a source of soil protection (McClaren, 1995). Attaining the ultimate goal of rangeland sustainability requires the monitoring of grassland condition, or its state of health. The National Research Council (1994) defined an organism as being healthy when it is "functioning properly and normally in its vital functions". Photosynthesis is a vital function of grasslands and has been used to monitor rangeland condition at fine scales using various closed, open, and isotopic systems (Field et al., 1989). Unfortunately, photosynthesis is very difficult to estimate at the regional scale.

A number of methods using satellite data have been developed to estimate regional evapotranspiration (EΓ), or transpiration in cases when evaporation (E) is zero (Boegh et al., 1999; 2000; Granger, 2000). Transpiration is directly related to photosynthesis because as plants open their stomates to take up carbon dioxide for photosynthesis, water is lost

C.D. Holifield,[1] S. McElroy, M.S. Moran, R. Bryant, and W.E. Emmerich. U.S. Department of Agriculture, Agricultural Research Service, Southwest Watershed Research Center, 2000 E. Allen Road, Tucson, AZ 85719, U.S.A.

T. Miura. Department of Soil, Water and Environmental Science, University of Arizona, Tucson, AZ 85721, U.S.A.

[1]Corresponding author (e-mail: cholifield@tucson.ars.ag.gov).

through transpiration. Due to this link with photosynthesis, transpiration can be used as an indicator of plant condition.

Images from satellite-based sensors have been used to monitor plant and soil conditions over extensive regions, particularly through estimation of EΓ. Most methods for estimation of rangeland EΓ from satellite imagery require a great deal of information about plant cover, plant height, and soil moisture, which is difficult to compute over a heterogeneous region (Foran, 1987; Graetz, 1987; Henebry, 1993; Ringrose et al., 1999). One approach, based on a combination of surface reflectance and temperature and meteorological data, has been successfully applied over heterogeneous terrain with little a priori information. This approach, termed the water deficit index (WDI) (Moran et al., 1996), was used in this study to give a relative estimate of EΓ over a considerable area (900 ha). In the southwest United States, where evaporation from soil is generally small due to infrequent rain events, estimates of EΓ are generally dominated by transpiration from plants. Thus, regional estimates of EΓ from satellites can be related directly to transpiration, and consequently to plant condition.

In the past, a temporal study like this one would have been limited to the lifespan of a single satellite sensor or would have involved the use of imagery from a combination of different satellite sensors (e.g., Landsat thematic mapper (TM), Satellite pour l'observation de la terre high-resolution visible (SPOT HRV), National Oceanic and Atmospheric Administration advanced very high resolution radiometer (NOAA AVHRR)). The 1999 launch of Landsat-7, however, provided the opportunity to utilize the imagery of sensors on board three consecutive Landsat satellites, Landsat-4 TM, Landsat-5 TM, and Landsat-7 enhanced thematic mapper plus (ETM+). The site for this study was the U.S. Department of Agriculture Walnut Gulch Experimental Watershed (WGEW) near Tombstone, Arizona, which has been the site for numerous remote sensing studies from 1990 to the present. The first step in the analysis was to retrieve surface reflectance and temperature from the Landsat image digital number (dn) and then compute WDI for the grassland regions of WGEW. The subsequent analysis of WDI for the 11-year period included (*i*) a comparison of Landsat-4 TM, Landsat-5 TM, and Landsat-7 ETM+; (*ii*) a comparison of the relation between WDI and grassland transpiration; (*iii*) an investigation of the temporal and spatial variability of WDI, related theoretically to changes in grassland transpiration; and (*iv*) an examination of the relationship between WDI and an antecedent retention index (ARI) used to estimate plant-available soil moisture.

Methods and data processing

The following subsections include the theory behind the WDI, some discussion about ARI and its computation, procedures that were involved in processing the satellite imagery, and a description of the study area and its instrumentation.

WDI theory

The WDI is based on a vegetation index – temperature (VIT) trapezoid (**Figure 1**) that combines a spectral vegetation index with surface temperature (combination of soil and vegetation temperatures) to determine water deficit conditions. In this case, the soil-adjusted vegetation index (SAVI) was the spectral vegetation index used. SAVI was calculated using the following equation:

$$\text{SAVI} = \frac{\rho_{\text{NIR}} - \rho_{\text{red}}}{(\rho_{\text{NIR}} + \rho_{\text{red}} + L)(1 + L)}, \tag{1}$$

where ρ_{NIR} and ρ_{red} are the near-infrared (NIR) and red reflectances, respectively; and L (soil adjustment constant) is assumed to be 0.5 for a variety of leaf area index (LAI) values (Huete, 1988).

The surface temperature minus air temperature $(T_s - T_a)$ values for the four vertices of the VIT trapezoid were defined by combining the Penman–Monteith equation (Monteith, 1973) with energy balance equations, as originally proposed by Jackson et al. (1981). The subscript n of $(T_s - T_a)_n$ refers to vertex n in **Figure 1**. Vertex 1 of the trapezoid represents full-cover, well-watered vegetation, and $(T_s - T_a)_1$ is computed as

$$(T_s - T_a)_1 = \frac{r_a(\boldsymbol{R}_n - \boldsymbol{G})}{C_v} \frac{\gamma\left(1 + \frac{r_{cp}}{r_a}\right)}{\Delta + \gamma\left(1 + \frac{r_{cp}}{r_a}\right)} \\ - \frac{\text{VPD}}{\Delta + \gamma\left(1 + \frac{r_{cp}}{r_a}\right)}, \tag{2}$$

where r_a is the aerodynamic resistance (s·m^{-1}), $\boldsymbol{R}_n$ is the net radiant heat flux density (W·m^{-2}), $\boldsymbol{G}$ is the soil heat flux density (W·m^{-2}), C_v is the volumetric heat capacity of air (J·°C^{-1}·m^{-3}), γ is the psychrometric constant (Pa·°C^{-1}), r_{cp} is the canopy resistance at potential evapotranspiration, Δ is the slope of the saturated vapor pressure – temperature relation (Pa·°C^{-1}), and VPD is the vapor pressure deficit of the air (Pa). Vertex 2 represents full-cover vegetation with no available water, and $(T_s - T_a)_2$ is computed as

$$(T_s - T_a)_2 = \frac{r_a(\boldsymbol{R}_n - \boldsymbol{G})}{C_v} \frac{\gamma\left(1 + \frac{r_{cx}}{r_a}\right)}{\Delta + \gamma\left(1 + \frac{r_{cx}}{r_a}\right)} \\ - \frac{\text{VPD}}{\Delta + \gamma\left(1 + \frac{r_{cx}}{r_a}\right)}, \tag{3}$$

where r_{cx} is the canopy resistance associated with nearly complete stomatal closure. Vertex 3 represents saturated bare soil, and $(T_s - T_a)_3$ is computed as

$$(T_s - T_a)_3 = \frac{r_a(R_n - G)}{C_v} \frac{\gamma}{\Delta + \gamma} - \frac{VPD}{\Delta + \gamma}. \tag{4}$$

Vertex 4 represents dry bare soil, and $(T_s - T_a)_4$ is computed as

$$(T_s - T_a)_4 = \frac{r_a(R_n - G)}{C_v}. \tag{5}$$

A more detailed description of how the inputs to Equations (2)–(5) can be defined and the limitations of the WDI were given by Moran et al. (1996).

The left and right sides of the trapezoid formed by the connection of vertices 1 and 3 and 2 and 4 are known as the cool and warm edges, respectively. The cool edge represents the theoretical range of $T_s - T_a$ for conditions of potential evapotranspiration ($E\Gamma_p$). The warm edge represents the theoretical range of $T_s - T_a$ when $E\Gamma = 0$. Therefore, when soil evaporation is close to zero, the WDI becomes a measure of transpiration (Γ) and has been defined as

$$WDI = 1 - \frac{\Gamma}{\Gamma_p}, \tag{6}$$

where Γ_p is potential transpiration. Theoretically, the WDI ranges from 0.0 for well-watered conditions to 1.0 for maximum stress conditions and graphically is equal to the ratio of distances AC and AB for a hypothetical measurement at point C in **Figure 1**. It should also be noted that as $E\Gamma_p$ varies, the vertex points of the VIT trapezoid will also vary in time and space.
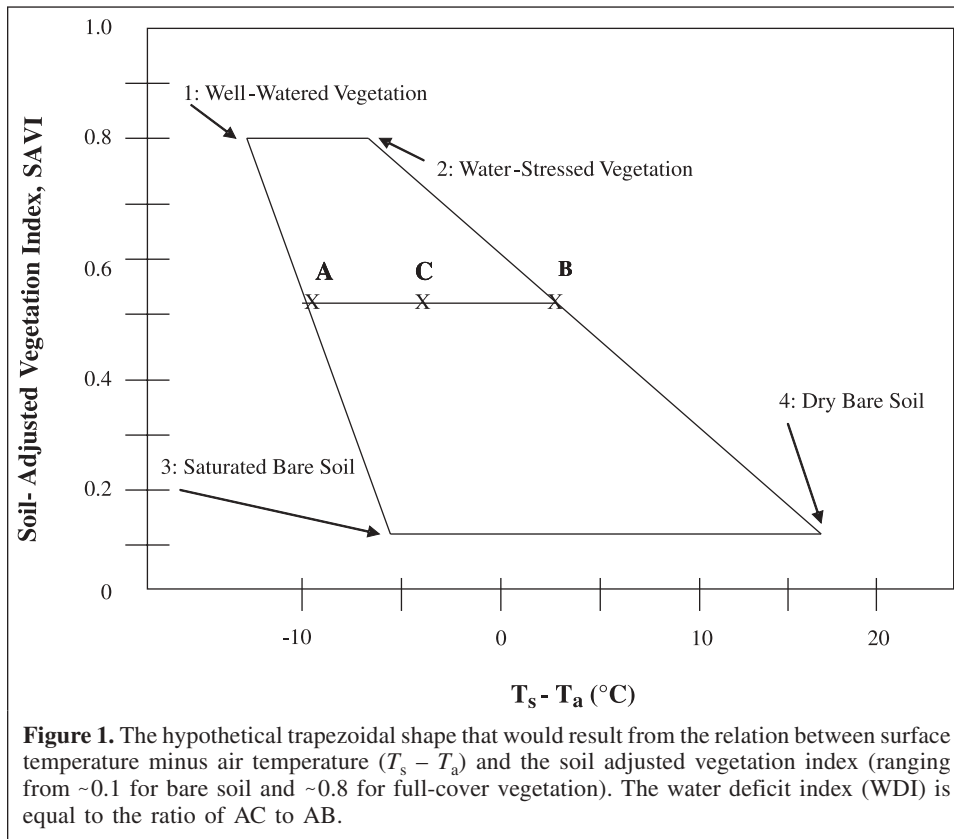
Antecedent retention index (ARI)

The antecedent retention index (ARI) (Saxton and Lenz, 1967) was used in this study to estimate plant-available soil moisture. ARI is based on antecedent precipitation minus runoff and accounts for soil water loss over time using the decay constant (K), which is based on soil type, as given by Saxton and Lenz (1967). In this study, all of the sites were dominated by soil classified as loamy upland – limy slopes, and a single constant of $K = 0.85$ was used. Thus, the equation used to calculate ARI was

$$ARI_i = (ARI_{i-1} + R_{i-1})K, \tag{7}$$

where R is the precipitation minus runoff, and i is the selected day.

The soil moisture information obtained from the ARI was compared with transpiration information estimated by the WDI. The proposed relation between ARI and WDI was based on an equation presented in Moran et al. (1997):

Figure 1. The hypothetical trapezoidal shape that would result from the relation between surface temperature minus air temperature ($T_s - T_a$) and the soil adjusted vegetation index (ranging from ~0.1 for bare soil and ~0.8 for full-cover vegetation). The water deficit index (WDI) is equal to the ratio of AC to AB.

$$1 - \frac{\Gamma}{\Gamma_p} = 1.17 e^{-12.91 h_v}, \tag{8}$$

where h_v is the volumetric soil moisture content. According to this equation, there is an exponential relationship between soil moisture (or, in our case, ARI) and relative transpiration rate (where WDI = $1 - \Gamma/\Gamma_p$).

Image processing

Changes in WDI were estimated using a 10-year (1990–1995 and 1997–2000) series of Landsat-4, Landsat-5, and Landsat-7 images of the WGEW in southeastern Arizona during the summer monsoon period (**Table 1**). These images were selected according to the criteria that no precipitation had occurred the day of or the day before the image was taken. This was done to ensure that the soil surface was dry at the time the image was taken, making the WDI an estimate of Γ rather than EΓ. Another requirement was that there was no precipitation the day following the image so that increases in humidity levels would not interfere with atmospheric correction. Each image was geocorrected to subpixel accuracy using the nearest neighbor resampling method. The refined empirical line (REL) method (Moran et al., 2001) was used to convert dn to reflectance for the green, red, and NIR spectral bands. The REL approach utilizes two points of known reflectance to determine a dn–reflectance relation for each spectral band on each date and was originally validated with data from WGEW (Moran et al., 2001).

Satellite-based surface temperatures (T_s) were retrieved from Landsat-4 and Landsat-5 TM dn according to the technique outlined by Lansing and Barker (1983) using the equation

$$T_s = \frac{K2}{\ln\left(\dfrac{K1}{\text{slope(dn)} + \text{offset} + 1}\right)} - \text{Kelvin}, \tag{9}$$

where slope = 0.005632, offset = 0.1238, and Kelvin = 273.15. For Landsat-5, K1 = 60.766 and K2 = 1260.56; for Landsat-4,

Table 1. List of Landsat images of the Walnut Gulch Experimental Watershed used for this study.

Landsat-4	Landsat-5	Landsat-7
4 Sept. 1991	24 Aug. 1990	26 Sept. 1999
	11 Oct. 1990	12 Sept. 2000
	14 Oct. 1991	28 Sept. 2000
	30 Sept. 1992	
	17 Sept. 1993	
	22 Oct. 1994	
	6 Aug. 1995	
	23 Sept. 1995	
	9 Oct. 1995	
	14 Oct. 1997	
	30 Aug. 1998	
	1 Oct. 1998	

K1 = 67.162 and K2 = 1284.3. For Landsat-7 ETM+, dn was converted to T_s using the equation

$$T_s = \frac{\dfrac{17.04}{254}(\text{dn} - 1)}{1000}, \tag{10}$$

provided by Schott et al. (2001). According to studies by Moran (1990), for typical clear sky conditions in Arizona, the difference between the surface temperature and the temperature measured above the atmosphere by the Landsat TM sensor was typically 2°C. Therefore, the temperatures computed from imagery using Equations (9) and (10) were increased by 2°C to account for atmospheric attenuation. These images of surface reflectance and temperature, and meteorological data acquired at the time and date of the satellite imagery, were used to compute the WDI according to Equations (2)–(6).

Previous studies have shown that reflectances retrieved from Landsat-4 TM, Landsat-5 TM, and Landsat-7 ETM+ can be combined with minimal error (Metzler and Malila, 1985; Price, 1989; Moran et al., 2001; Vogelmann et al., 2001). The TM and ETM+ on-board thermal calibration systems are essentially the same (Barker, 1985), and the calibrations of the Landsat TM and ETM+ thermal sensors have been remarkably stable (Schott et al., 2001), resulting in reliable estimates of at-satellite temperature based on published calibration factors. These studies provide confidence in the image-processing approaches used here for multisensor temporal analysis.
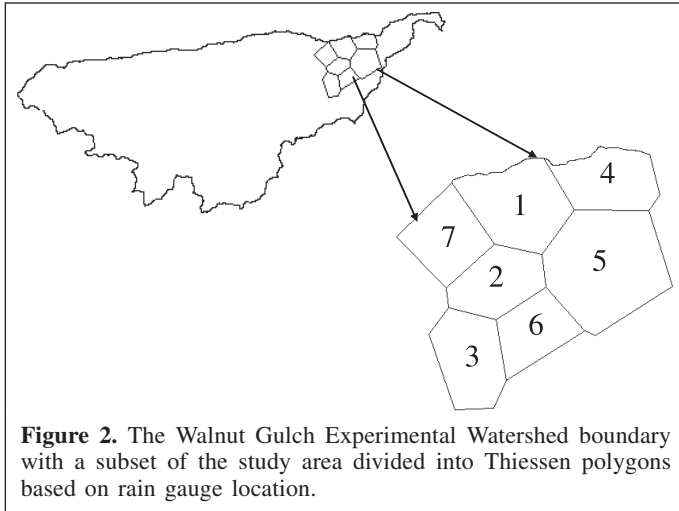
Study area and instrumentation

The Walnut Gulch Experimental Watershed (WGEW) encompasses 150 square kilometres and is representative of approximately 60 million hectares of brush- and grass-covered rangeland found throughout the semiarid southwestern United States (Renard et al., 1993). The lower two thirds of the watershed is dominated by desert shrub species, which transition into desert grasslands on the upper portion of the watershed.

An area of approximately 9 square kilometres located in the northeastern section of the watershed was examined for this study. This section of the watershed is dominated by black grama (*Bouteloua eriopoda*), blue grama (*Bouteloua gracilis*), sideoats grama (*Bouteloua curtipendula*), bush muhly (*Muhlenbergia porteri*), and Lehmann lovegrass (*Eragrostis lehmanniana*). The primary drainage runs from the northeast to the southwest. Typical ridge to valley height ranges from 15 to 20 m, and spacing between ridge tops is around 500 m.

To obtain a realistic estimate of available soil moisture and rainfall, the study area was divided into seven sections using Thiessen polygons based on the locations of rain gauges (**Figure 2**). The Thiessen method of determining areal rainfall assumes that at any point in the watershed the rainfall is the same as that of the nearest gauge. Polygon boundaries are formed by perpendicularly bisecting the lines joining adjacent gauges (Chow et al., 1988). Thiessen polygons divide a region based on the configuration of data points (i.e., rain gauges),

Figure 2. The Walnut Gulch Experimental Watershed boundary with a subset of the study area divided into Thiessen polygons based on rain gauge location.

with one observation per cell (Burrough and McDonnell, 1998).

Large and small flumes designed to measure runoff from rainfall events are located in the watershed (Renard et al., 1993). One such flume, located near the study area, was used with precipitation data from the rain gauges to estimate plant-available soil moisture using ARI.

This study also utilized data collected by Bowen ratio energy balance (BREB) instrumentation located in the watershed (Emmerich, 2002). With a fetch of 200+ m in all directions, these systems measure temperature, moisture, and CO_2 gradients every 2 s, average these measurements every 20 min, and store them in a datalogger. $E\Gamma$ and CO_2 flux values are then calculated for each 20-min period. Data from the BREB system located in study polygon 6 were used to determine an in situ measurement of $1 - \Gamma/\Gamma_p$.

To obtain a value for Γ_p, the day with the highest CO_2 uptake at 10:20 a.m., 10:40 a.m., and 11:00 a.m. was determined. These times were selected due to their proximity to the time of the satellite overpasses (mid-morning). A criterion of no precipitation the day before the day of highest CO_2 uptake also had to be met. Further, incoming solar radiation was examined to ensure that no clouds were present on the chosen day. August 13, 1999 (day of year (DOY) 225) met the criteria and was selected. The $E\Gamma$ measurements for DOY 225 at the times mentioned previously were used for Γ_p. Values for Γ were obtained from the $E\Gamma$ measurements for 5 days (DOY 287, DOY 242, DOY 274, DOY 256, and DOY 272) at the time of the satellite overpass. In situ transpiration values were calculated for each day using the appropriate Γ and Γ_p values. These values were used for a comparison of in situ transpiration measurements and WDI.

Results and discussion

The use of three Landsat sensors to conduct an analysis over an 11-year period provided the unique opportunity to investigate the temporal behavior of WDI through a single

growing season (1995) and over multiple seasons characterized by wet and dry conditions. The choice of the well-instrumented WGEW for the study site allowed access to a network of on-site instrumentation and a heterogeneous grassland for spatial studies. The results of this analysis include a comparison of Landsat-4 TM, Landsat-5 TM, and Landsat-7 ETM+, confirmation of the relationship between WDI and grassland Γ, investigation of WDI for monitoring grassland variability, and a study of the relation between WDI and ARI.

Comparison of Landsat-4 TM, Landsat-5 TM, and Landsat-7 ETM+

Since this study combined images from three sensors over an 11-year period to investigate temporal surface changes, it was imperative that retrieval of surface reflectance and temperature from image dn accounted for both atmospheric and sensor differences. As mentioned in the Methods and data processing section, previous studies had shown that reflectance and temperature could be retrieved from the Landsat TM and ETM+ sensors with minimal between-sensor error. Though this study was not designed to determine the error associated with combining multisensor reflectance and temperature measurements, our data set provided qualitative support for the positive findings of previous studies.

First, we compared the surface reflectances retrieved for the seven study polygons from Landsat-4 TM and Landsat-5 TM images acquired, respectively, in September (DOY 247) and October (DOY 287) in 1991. Theoretically, the grassland should have senesced between the September and October acquisitions, resulting in a decrease in the green and NIR reflectance and an increase in the red reflectance. This was supported by data for all seven polygons and is illustrated for polygon 7 in **Figure 3**.
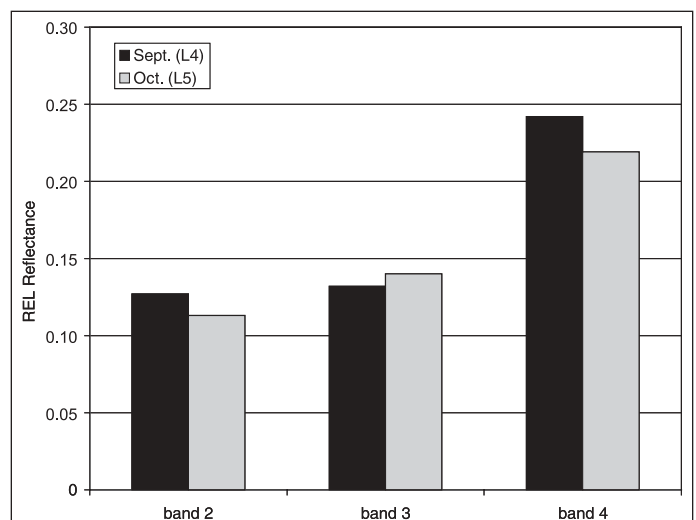
Figure 3. Comparison of reflectances of TM spectral bands 2 (green), 3 (red), and 4 (NIR) calculated using the refined empirical line (REL) approach for Landsat-4 (L4, 4 Sept. 1991, DOY 247) and Landsat-5 (L5, 14 Oct. 1991, DOY 287) images for study polygon 7.

We also compared reflectances retrieved from the Landsat-5 TM and Landsat-7 ETM+ dn using the REL approach, with reflectances retrieved from the same dn in previous studies using a more conventional approach. In the conventional approach, we measured atmospheric optical depth with a solar radiometer and used these data in a radiative transfer model to compute the surface reflectance for a given at-satellite radiance (e.g., Thome, 2001). This data set was used to confirm that the REL-derived reflectances were similar to those derived using an independent, more complex approach for both sensors. The mean absolute difference (MAD) of SAVI calculated using reflectances retrieved with the two methods for four dates was 0.03. This magnitude of error met the requirements for computation of WDI.

Unlike surface reflectance, surface temperature varies dramatically day-to-day depending on climatic conditions and surface soil moisture. As a result, it is difficult to determine the absolute accuracy of temperatures retrieved from the Landsat sensor dn without spatially and temporally coincident surface temperature measurements. Some confidence in T_s measurements was attained simply by the fact that very few $T_s - T_a$ values for the study area exceeded the cool and warm edges of the VIT trapezoid, and in the cases when this did occur the difference was less than 1°C. Furthermore, there were no distinct trends in the T_s values that could be attributed solely to retrieval from the Landsat-4, Landsat-5, or Landsat-7 sensors.

Based on these qualitative comparisons, there were no distinguishable differences in reflectances and temperatures derived from Landsat-4, Landsat-5, or Landsat-7 satellite images. The data continuity among all three satellites appeared suitable for computing WDI. A more formal study of the data continuity of the Landsat-4 TM, Landsat-5 TM, and Landsat-7

ETM+ visible, NIR, and short-wavelength infrared (SWIR) spectral bands, with reference to WGEW, was presented by Bryant et al. (2002).
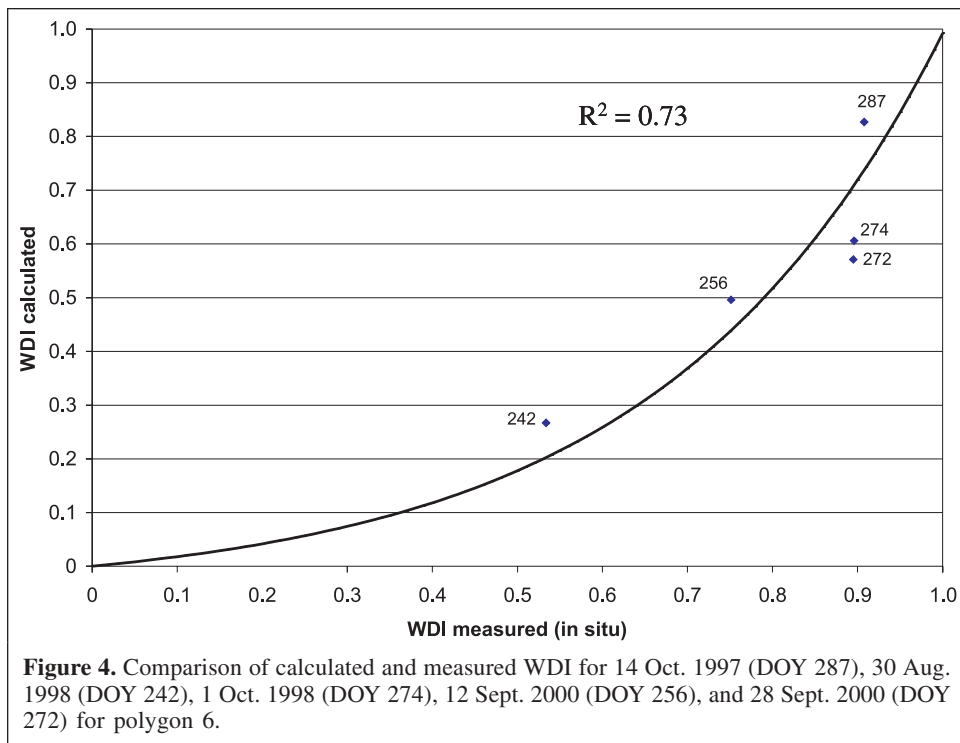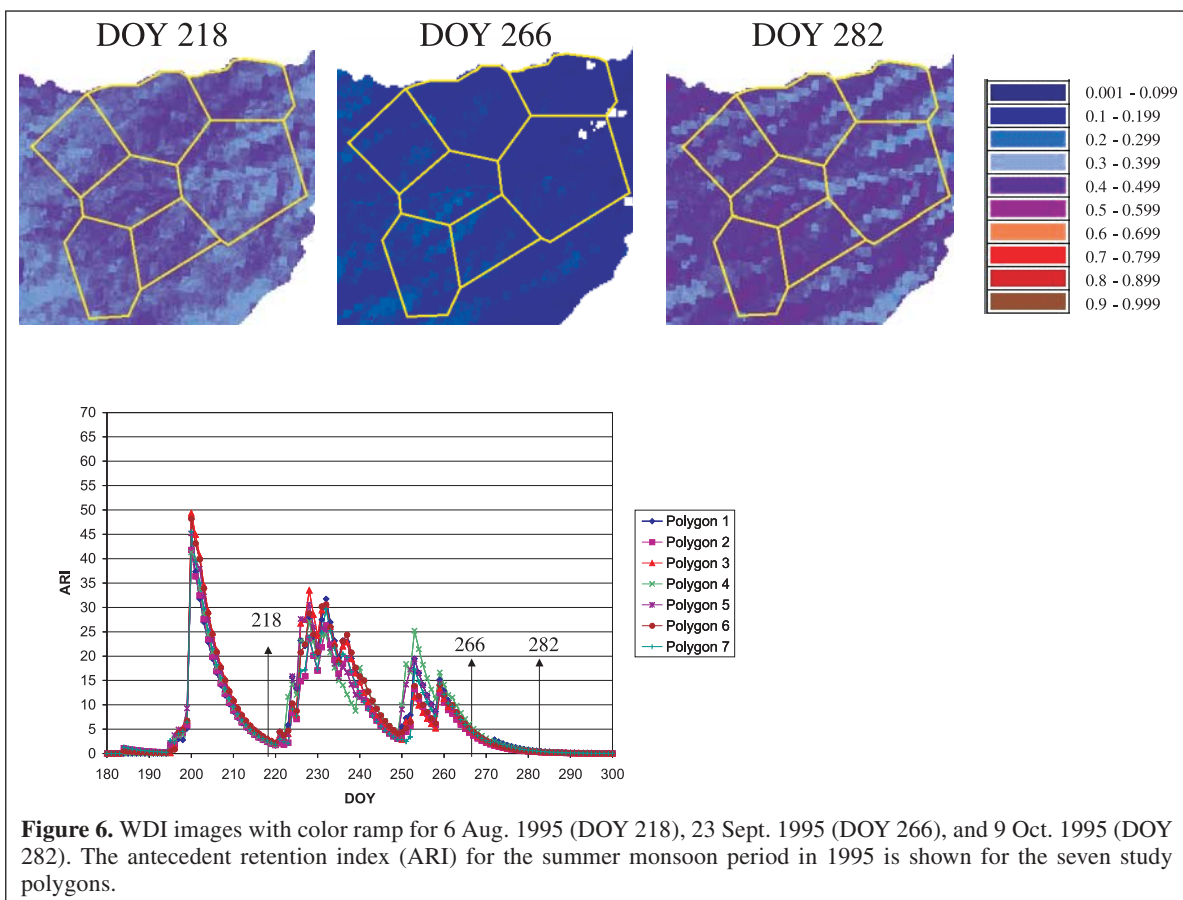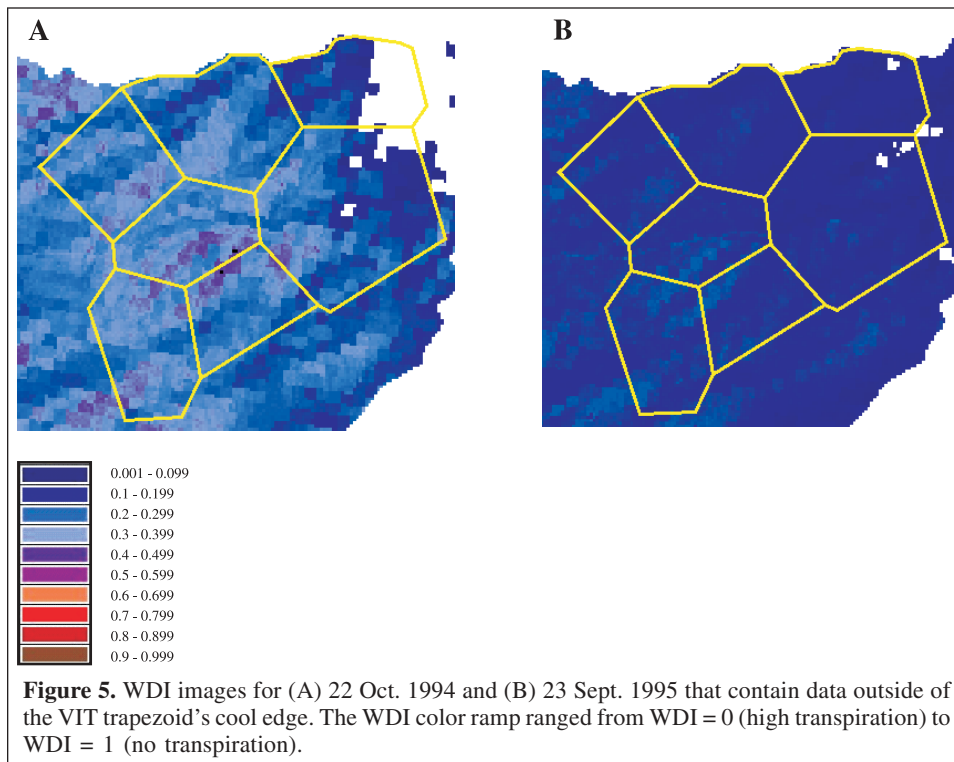
Relation between WDI and grassland transpiration

A first step in this analysis was to confirm that WDI = 1 – Γ/Γ_p. This relation was validated by Moran et al. (1996) for a ground-based data set at WGEW. In this study, transpiration rates measured with a BREB system during the growing season (1 July – 31 October) for 1997–2000 were used for the analysis. The in situ data were compared with the WDI data for study polygon 6 and are shown in **Figure 4**.

An exponential relationship was found, as predicted theoretically by Moran et al. (1994). The relationship is exponential because WDI does not account for sensible heat transfer between warm soil and cool vegetation that results in an increase in canopy Γ when surface heterogeneity is greatest (partial-cover vegetation cover conditions). However, considering the differences in scale and the potential error in both measurement approaches, the relation is good (correlation coefficient $R^2 = 0.73$) and supports the use of WDI for monitoring grassland transpiration.

Investigation of WDI for monitoring grassland variability

A color ramp was applied to all images to depict the WDI values throughout the study area. Two of the images had white areas associated with them (**Figure 5**) due to the fact that some of the measured values of $T_s - T_a$ slightly exceeded the cool or warm edges of the VIT trapezoid, causing WDI to be less than zero or greater than 1.0. Such discrepancies could be caused by

Figure 4. Comparison of calculated and measured WDI for 14 Oct. 1997 (DOY 287), 30 Aug. 1998 (DOY 242), 1 Oct. 1998 (DOY 274), 12 Sept. 2000 (DOY 256), and 28 Sept. 2000 (DOY 272) for polygon 6.

Figure 5. WDI images for (A) 22 Oct. 1994 and (B) 23 Sept. 1995 that contain data outside of the VIT trapezoid's cool edge. The WDI color ramp ranged from WDI = 0 (high transpiration) to WDI = 1 (no transpiration).

Figure 6. WDI images with color ramp for 6 Aug. 1995 (DOY 218), 23 Sept. 1995 (DOY 266), and 9 Oct. 1995 (DOY 282). The antecedent retention index (ARI) for the summer monsoon period in 1995 is shown for the seven study polygons.

error in the satellite sensor calibration, overcorrection or undercorrection of the remotely sensed data for atmospheric conditions, or errors associated with calculating the warm and cool edges (Equations (2)–(5)). More discussion of the magnitude of these errors was given by Moran et al. (1994).

The WDI detected both temporal and spatial variations in grasslands at WGEW. The temporal variation was illustrated by ARI and WDI data from three images (DOY 218, DOY 266, and DOY 282) acquired during the 1995 summer monsoon season (**Figure 6**). The decrease in WDI (i.e., increase in transpiration) of approximately 0.3 from DOY 218 to DOY 266 was due to an increase in precipitation within that 48-day period. Following this interval, an increase in WDI of approximately 0.3 was detected between DOY 266 and DOY 282 due to the soil drying out over a 16-day period. Thus, the 1995 data illustrated the changes in transpiration caused by an increase, and subsequent decrease, in ARI and, consequently, plant-available soil moisture.

The sensitivity of the WDI to variations in grasslands due to variable antecedent rainfall was demonstrated with data from an image obtained on 30 August 1998 (DOY 242) (**Figure 7**). On DOY 236, an intense but localized rain storm swept through WGEW. Precipitation amounts of up to 25 mm were measured in the western polygons of our study area, and amounts of less than 2 mm were measured in the eastern polygons. This difference was reflected in ARI values, ranging from 18 in the western polygons to 4 in the eastern polygons. The WDI illustrated a similar trend, ranging from 0.22 in the western polygons to 0.38 in the eastern polygons. Though the WDI calculations (Equations (2)–(6)) were independent of precipitation measurements, WDI offered a distributed indication of the precipitation pattern based on plant transpiration rates 6 days after the storm.

The WDI was also sensitive to changes in grasslands induced by topographic differences (**Figures 8** and **9**). Grassland transpiration was higher on north-facing slopes (and thus WDI was lower) due to the fact that slopes with these aspects retain soil moisture longer than slopes with southern aspects (Qiu et al., 2001). This was illustrated by WDI values extracted from north- and south-facing slopes on four dates, for which WDI values ranged from very low (DOY 269) to very high (DOY 274). Regardless of the overall magnitude of WDI for the study site, the difference between WDI values extracted from north- and south-facing slopes on any given day was always apparent (**Figure 9**). Based on the greater standard deviations of values extracted from areas with north-facing slopes, it appeared that greater variability in WDI, and thus plant transpiration rates, existed on north-facing slopes than on south-facing slopes. To further quantify the differences between north- and south-facing slopes shown in **Figure 9**, a one-way analysis of variance across all four dates was performed. The result indicated that the south-facing slopes had significantly (significance level $P < 0.05$) higher WDI values than north-facing slopes across all dates.

Relation between WDI and ARI

The WDI and ARI data from all 10 years and seven study polygons ($n = 112$) were combined to investigate the relation between WDI and ARI. Assuming the relation would be exponential (Equation (8)), the following relation was determined (**Figure 10**):

$$WDI = 0.62e^{-0.103ARI} \tag{11}$$

This relation was significant but weak ($R^2 = 0.45$). There were several factors that could account for this discrepancy. The first might be errors in WDI due to the numerous inputs required to compute the trapezoid (Equations (2)–(5)). For example, for our data set an error of 1°C in surface or air temperature resulted in a 13–17% difference in the WDI calculation. A second factor was the error associated with the inputs used in the generation of the ARI, including rainfall, runoff, and the choice of the K coefficient. A third factor was associated with a little understood divergence in the data for years 1994 and 1995. The points scattered in the lower left corner of **Figure 10** are all associated with these 2 years; all other years followed the exponential relation quite well. If data from 1994 and 1995 were excluded from the analysis, the ARI–WDI relation would have been much stronger ($R^2 = 0.77$). After investigation of the sensor stability, meteorological data, dn-to-reflectance conversion, WDI inputs, and precipitation data, we were unsuccessful in determining the cause of this deviation from the trend.

Lastly, it should be noted that although WDI and ARI are both associated with available soil water, they are not measuring the same information. ARI is a measure of soil water content, whereas WDI is a measure of plant transpiration rate (Equation (6)). The data showed that a WDI value of approximately 0.6 was equivalent to an ARI value of zero. After this point, WDI continued to be responsive to changing conditions while ARI did not, implying that WDI was the more sensitive indicator of vegetation condition. By focusing on plant dynamics rather than simply available soil water, it is possible to account for differences in meteorological conditions, rooting depth, and plant physiological constraints.

Concluding remarks

The combination of Landsat-4 TM, Landsat-5 TM, and Landsat-7 ETM+ is a powerful source of information for temporal studies of natural resources. Our study showed that measurements of surface reflectance and temperature from the three sensors could be combined without sacrificing product accuracy. These results support the cross-calibration studies of Schott et al. (2001) and Bryant et al. (2002).

The water deficit index (WDI) derived from continuous Landsat-4, Landsat-5, and Landsat-7 imagery was useful for mapping temporal and spatial grassland variability and topographically induced vegetation differences. It appeared to be a more sensitive index than the antecedent retention index
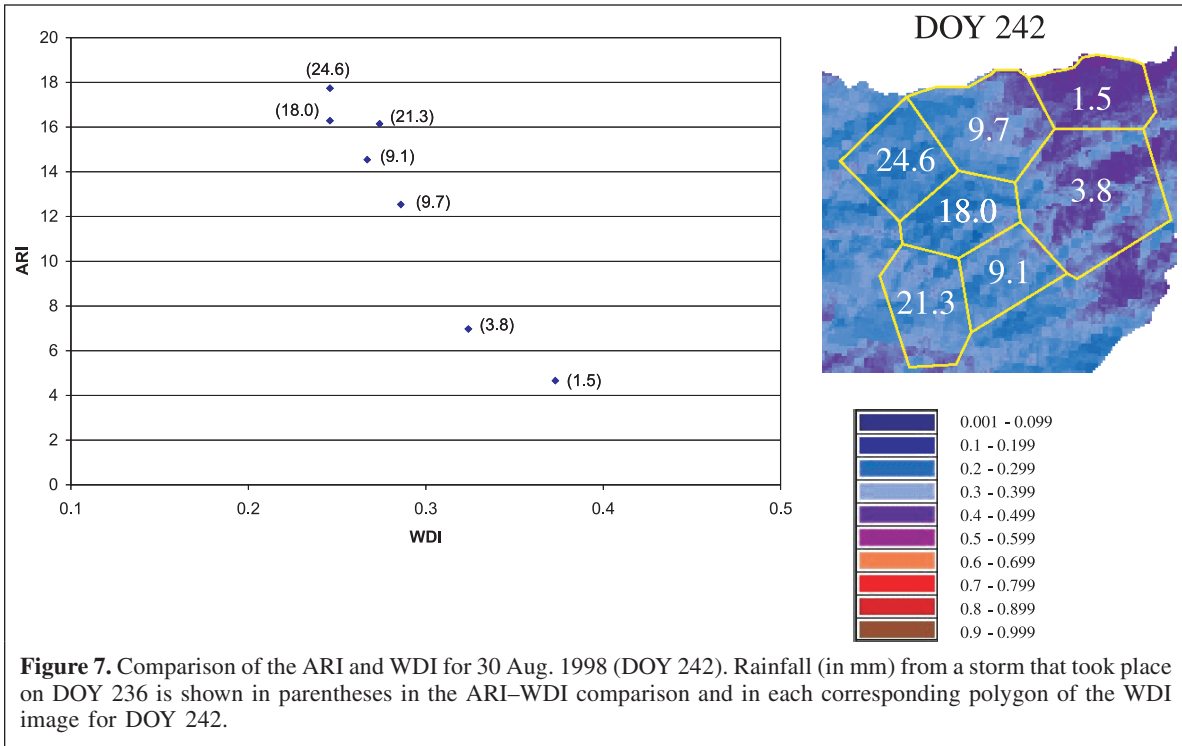
Figure 7. Comparison of the ARI and WDI for 30 Aug. 1998 (DOY 242). Rainfall (in mm) from a storm that took place on DOY 236 is shown in parentheses in the ARI–WDI comparison and in each corresponding polygon of the WDI image for DOY 242.
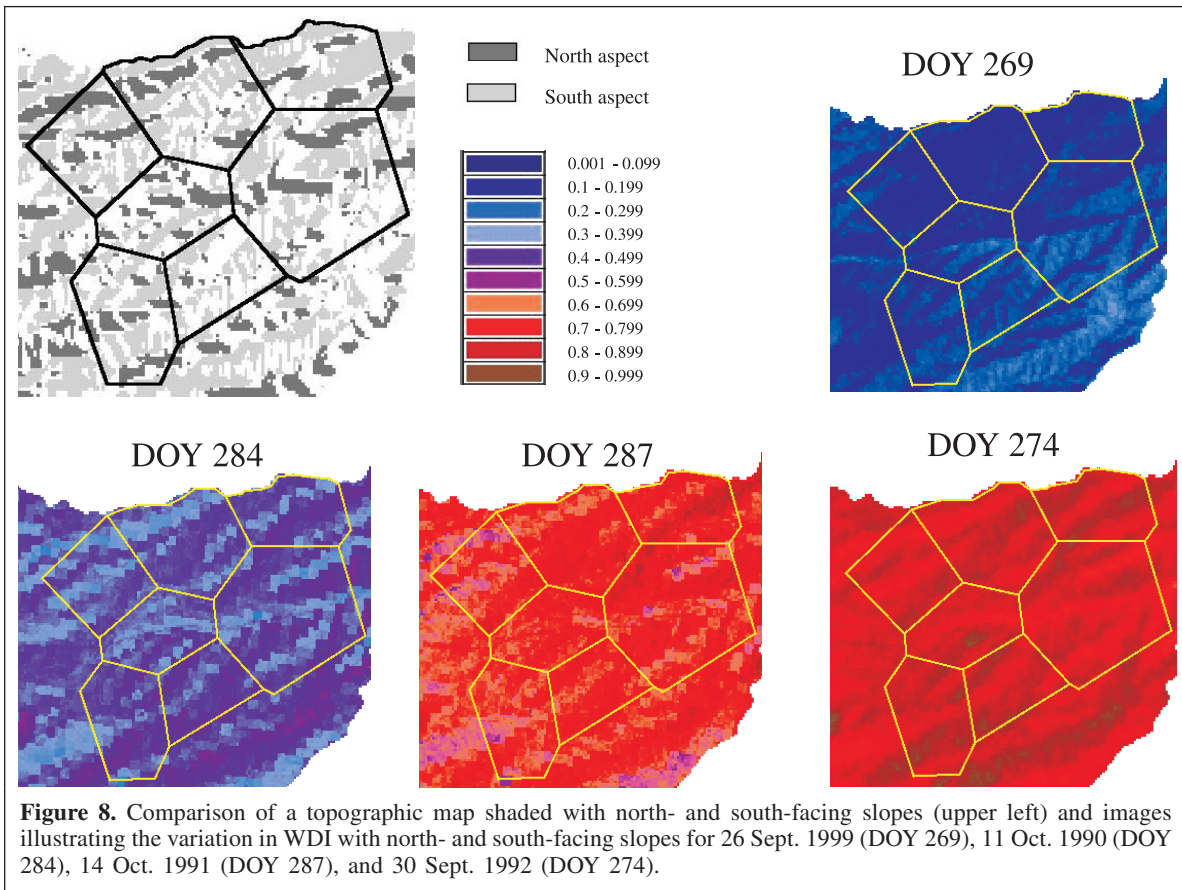

Figure 8. Comparison of a topographic map shaded with north- and south-facing slopes (upper left) and images illustrating the variation in WDI with north- and south-facing slopes for 26 Sept. 1999 (DOY 269), 11 Oct. 1990 (DOY 284), 14 Oct. 1991 (DOY 287), and 30 Sept. 1992 (DOY 274).

(ARI) for monitoring grassland water status. The WDI has advantages over ARI as a monitoring tool, including a

distributed rather than point-based product and more standard inputs (available from local meteorological stations rather than
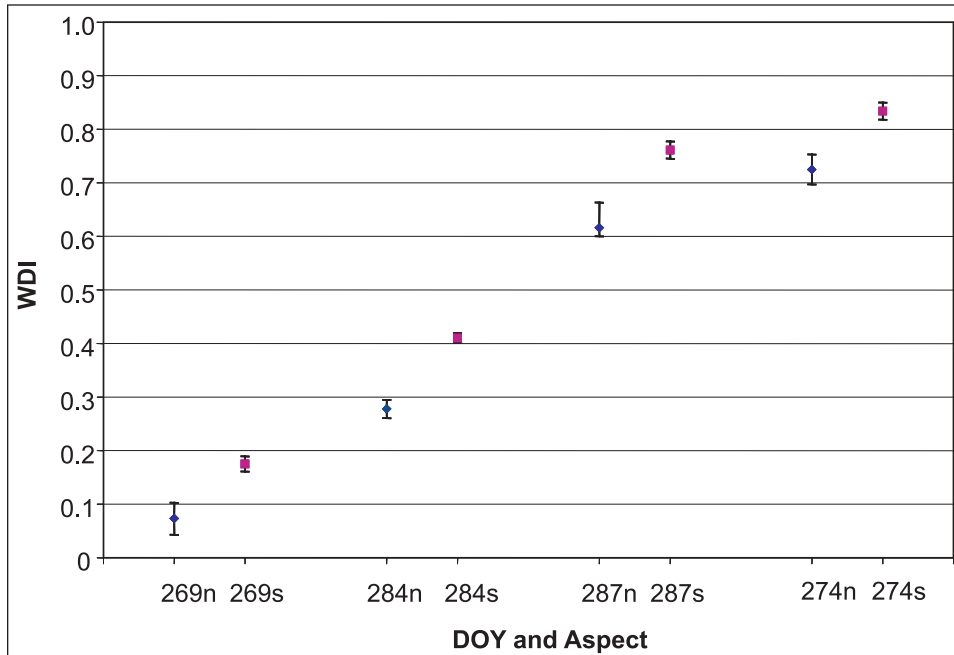
Figure 9. Comparison of means and standard deviations of WDI from selected north-facing (n) and south-facing (s) slopes for 26 Sept. 1999 (DOY 269), 11 Oct. 1990 (DOY 284), 14 Oct. 1991 (DOY 287), and 30 Sept. 1992 (DOY 274). Standard deviations range from 0.01 to 0.05.
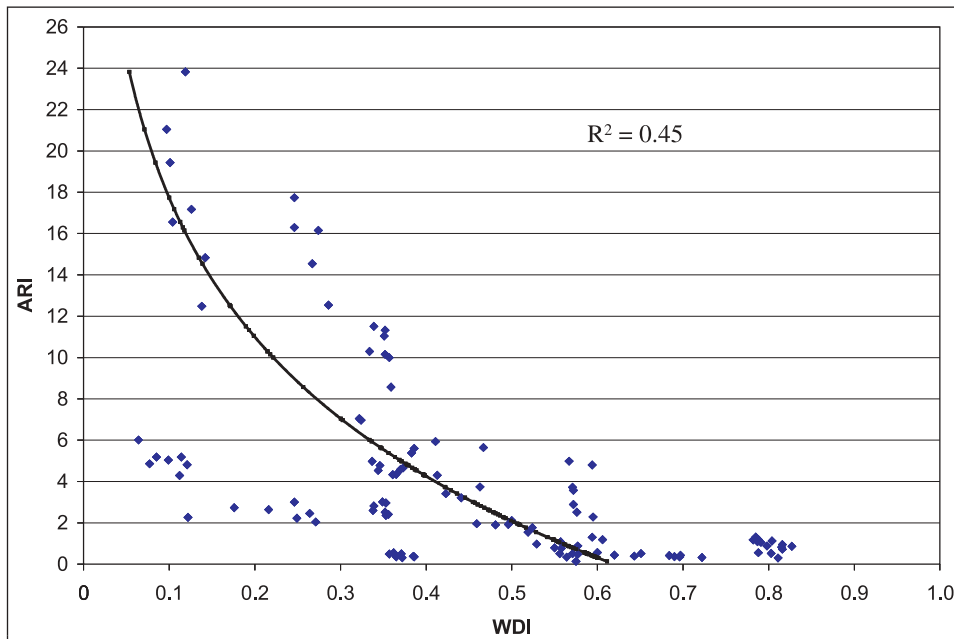
Figure 10. Comparison of ARI and WDI for 10 years for the seven study polygons. The solid line represents the regression fit for the data.

from a rain-gauge and runoff instrumentation network). A possible disadvantage of WDI is that it can only be computed at the time of the satellite overpass (mid-morning in the case of Landsat), which is not necessarily the time of maximum plant water deficit.

This study showed the WDI to be a viable tool for monitoring relative plant condition over heterogeneous semiarid grasslands. However, there are two main drawbacks to

operational use of the WDI for monitoring plant condition: (*i*) it is a point-in-time measurement (approx. 10:30 a.m.), not a measure of daily stress; and (*ii*) it is very difficult to obtain images during the growing season. The satellite makes repeat visits of a single site every 16 days, and the images are often unacceptable due to cloud interference. In our case, for an 11-year period, we were only able to obtain 16 images that fit our criteria. This could be overcome by supplementing intermittent

WDI images with temporally continuous simulation modeling to provide information for critical periods when satellite data are not available (e.g., Nouvellon et al., 2001). Future work should be directed to quantify and reduce the error associated with inputs used for the WDI calculation, which would strengthen this prospective rangeland management tool.

Acknowledgements

References

Barker, J.L. (Editor). 1985. *Proceedings of the Landsat-4 Science Characterizations Early Results Symposium*, February 1983, Greenbelt, Md. NASA Conference Publication CP-2355, U.S. National Aeronautics and Space Administration, Washington, D.C.

Boegh, E., Soegaard, H., Hanan, N., Kabat, P., and Lesch, L. 1999. A remote sensing study of the NDVI–T_s relationship and the transpiration from sparse vegetation in the Sahel based on high-resolution satellite data. *Remote Sensing of Environment*, Vol. 69, pp. 224–240.

Boegh, E., Shelde, K., and Soegaard, H. 2000. Estimating transpiration rates in a Danish agricultural area using Landsat thermal mapper data. *Physics and Chemistry of the Earth: Part B, Hydrology, Oceans and Atmosphere*, Vol. 25, Nos. 7–8, pp. 685–689.

Bryant, R., Moran, M.S., McElroy, S., Holifield, C., Thome, K., and Miura, T. 2002. Data continuity of Landsat-4 TM, Landsat-5 TM, Landsat-7 ETM+, and advanced land imager (ALI) sensors. *IEEE Transactions of Geoscience and Remote Sensing*. In press.

Burrough, P.A., and McDonnell, R.A. 1998. Creating continuous surfaces from point data. In *Principles of geographical information systems*. Oxford University Press, New York. p. 114.

Chow, V.T., Maidment, D.R., and Mays, L.W. 1988. Atmospheric water. In *Applied hydrology*. McGraw-Hill, Inc., New York. p. 78.

Emmerich, W.E. 2002. Carbon dioxide fluxes in a semiarid environment with high carbonate soils. *Agricultural and Forest Meteorology*, Vol. 3105, pp. 1–12.

Field, C.B., Ball, J.T., and Berry, J.A. 1989. Photosynthesis: principles and field techniques. In *Plant physiological ecology: field methods and instrumentation*. Edited by R.W. Pearcy, J. Ehleringer, H.A. Mooney, and P.W. Rundel. Chapman & Hall, London. p. 210.

Foran, B.D. 1987. Detection of yearly cover change with Landsat MSS on pastoral landscapes in central Australia. *Remote Sensing of Environment*, Vol. 23, pp. 333–350.

Graetz, R.D. 1987. Satellite remote sensing of Australian rangelands. *Remote Sensing of Environment*, Vol. 23, pp. 313–331.

Granger, R.J. 2000. Satellite-derived estimates of evapotranspiration in the Gediz Basin. *Journal of Hydrology*, Vol. 229, pp. 70–76.

Henebry, G.M. 1993. Detecting change in grasslands using measures of spatial dependence with Landsat TM data. *Remote Sensing of Environment*, Vol. 46, pp. 223–234.

Huete, A.R. 1988. A soil-adjusted vegetation index (SAVI). *Remote Sensing of Environment*, Vol. 27, pp. 47–57.

Jackson, R.D., Idso, S.B., Reginato, R.J., and Pinter, P.J., Jr. 1981. Canopy temperature as a crop water stress indicator. *Water Resources Research*, Vol. 17, pp. 1133–1138.

Lansing, J.C., and Barker, J.L. 1983. Thermal band characterization of the Landsat-4 thematic mapper. In *Proceedings of the Landsat-4 Science Characterizations Early Results Symposium*, February 1983, Greenbelt, Md. Edited by J.L. Barker. NASA Conference Publication CP-2355, U.S. National Aeronautics and Space Administration, Washington, D.C.

McClaren, M.P. 1995. Desert grasslands and grasses. In *The desert grassland*. Edited by M.P. McClaren and T.R. Van Devender. The University of Arizona Press, Tucson, Ariz. p. 3.

Metzler, M.D., and Malila, W.A. 1985. Characterization and comparison of Landsat-4 DN Landsat-5 thematic mapper data. *Photogrammetric Engineering and Remote Sensing*, Vol. 51, pp. 1315–1330.

Monteith, J.L. 1973. *Principles of environmental physics*. Arnold, London.

Moran, M.S. 1990. *A satellite-based approach for evaluation of the spatial distribution of evapotranspiration from agricultural lands*. Ph.D. dissertation, Department of Soil and Water Science, University of Arizona, Tucson, Ariz. 223 pp.

Moran, M.S., Clarke, T.R., Inoue, Y., and Vidal, A. 1994. Estimating crop water deficit using the relation between surface-air temperature and spectral vegetation index. *Remote Sensing of Environment*, Vol. 49, pp. 246–263.

Moran, M.S., Rahman, A.F., Washburne, J.C., Goodrich, D.C., Weltz, M.A., and Kustas, W.P. 1996. Combining the Penman–Monteith equation with measurements of surface temperature and reflectance to estimate evaporation rates of semiarid grassland. *Agricultural and Forest Meteorology*, Vol. 80, pp. 87–109.

Moran, M.S., Vidal, A., Troufleau, D., Qi, J., Clarke, T.R., Pinter, P.J., Jr., Mitchell, T.A., Inoue, Y., and Neale, C.M.U. 1997. Combining multifrequency microwave and optical data for crop management. *Remote Sensing of Environment*, Vol. 61, pp. 96–109.

Moran, M.S., Bryant, R., Thome, K., Ni, W., Nouvellon, Y., Gonzalez-Dugo, M.P., Qi, J., and Clarke, T.R. 2001. A refined empirical line approach for reflectance factor retrieval from Landsat-5 TM and Landsat-7 ETM+. *Remote Sensing of Environment*, Vol. 78, pp. 71–82.

National Research Council. 1994. Rangeland health. In *Rangeland health: new methods to classify, inventory, and monitor rangelands*. National Academy Press, Washington, D.C. p. 35.

Nouvellon, Y., Moran, M.S., Lo Seen, D., Bryant, R.B., Ni, W., Begue, A., Chehbouni, A.G., Emmerich, W.E., Heilman, P., and Qi, J. 2001. Coupling a grassland ecosystem model with Landsat imagery for a 10-year simulation of carbon and water budgets. *Remote Sensing of Environment*, Vol. 78, pp. 131–149.

Price, J.C. 1989. Calibration comparison for the Landsat 4 and 5 multispectral scanners and thematic mappers. *Applied Optics*, Vol. 28, pp. 465–471.

Qiu, Y., Chen, L., Fu, B., and Wang, J. 2001. Soil moisture variation in relation to topography and land use in a hillslope catchment of the Loess Plateau, China. *Journal of Hydrology*, Vol. 240, Nos. 3–4, pp. 243–263.

Renard, K.G., Lane, L.J., Simanton, J.R., Emmerich, W.E., Stone, J.J., Weltz, M.A., Goodrich, D.C., and Yakowitz, D.S. 1993. Agricultural impacts in an arid environment: Walnut Gulch studies. *Hydrological Science and Technology*, Vol. 9, pp. 145–190.

Ringrose, S., Musisi-Nkambwe, S., Coleman, T., Nellis, D., and Bussing, C. 1999. Use of Landsat thematic mapper data to assess seasonal rangeland changes in the southeast Kalahari, Botswana. *Environmental Management*, Vol. 23, No. 1, pp. 125–138.

Saxton, K.E., and Lenz, A.T. 1967. Antecedent retention indexes predict soil moisture. *ASCE Journal of the Hydraulics Division*, Vol. 93, No. HY4, pp. 223–241.

Schott, J.R., Barsi, J.S., Nordgren, B.L., Raqueno, N.G., and de Alwis, D. 2001. Calibration of Landsat thermal data and application to water resource studies. *Remote Sensing of Environment*, Vol. 78, pp. 108–117.

Thome, K.J. 2001. Absolute radiometric calibration of Landsat-7 ETM+ using the reflectance-based method. *Remote Sensing of Environment*, Vol. 78, pp. 27–38.

Vogelmann, J.E., Helder, D., Morfitt, R., Choate, M.J., Merchant, J.W., and Bulley, H. 2001. Effects of Landsat 5 Thematic Mapper and Landsat 7 enhanced thematic mapper plus radiometric and geometric calibrations and corrections on landscape characterization. *Remote Sensing of Environment*, Vol. 78, pp. 55–70.

List of symbols

ARI antecedent retention index

BREB Bowen ratio energy balance

C_v volumetric heat capacity of air (J·°C^{-1}·m^{-3})

dn digital number

DOY day of year

E evaporation

EΓ evapotranspiration

EΓ$_p$ potential evapotranspiration

G soil heat flux density (W·m^{-2})

h_v volumetric soil moisture content (cm^3·cm^{-3})

i selected day

K ARI decay constant

L soil adjustment constant

LAI leaf area index

MAD mean absolute difference

n vertex

P significance level

r_a aerodynamic resistance (s·m^{-1})

r_{cp} canopy resistance at potential evapotranspiration

r_{cx} canopy resistance associated with nearly complete stomatal closure

R precipitation minus runoff

R^2 correlation coefficient

R_n net radiant heat flux density (W·m^{-2})

SAVI soil adjusted vegetation index

T_a air temperature (°C)

T_s satellite-based surface temperature (°C)

VIT vegetation index – temperature

VPD vapor pressure deficit (Pa)

WDI water deficit index

Δ slope of the saturated vapor pressure – temperature relation (Pa·°C^{-1})

Γ transpiration

Γ_p potential transpiration

γ psychrometric constant (Pa·°C^{-1})

ρ_{NIR} near-infrared reflectance

ρ_{red} red reflectance